Snow accumulation variability on a West Antarctic ice stream observed with GPS reflectometry, 2007–2017

M. R. Siegfried[1,2], B. Medley[3], K. M. Larson[4], H. A. Fricker[1], S. Tulaczyk[5]

M. R. Siegfried, siegfried@stanford.edu

[1]Institute of Geophysics and Planetary Physics, Scripps Institution of Oceanography, University of California, San Diego, La Jolla, CA, USA.

[2]Department of Geophysics, Stanford University, Stanford, CA, USA.

[3]Cryospheric Sciences Laboratory, NASA Goddard Space Flight Center, Greenbelt, MD, USA.

[4]Department of Aerospace Engineering Sciences, University of Colorado, Boulder

This article has been accepted for publication and undergone full peer review but has not been through the copyediting, typesetting, pagination and proofreading process, which may lead to differences between this version and the Version of Record. Please cite this article as doi: 10.1002/2017GL074039

Land-ice loss from Antarctica is a significant and accelerating contribution to global sea-level rise; however, Antarctic mass-balance estimates are complicated by insufficient knowledge of surface mass-balance processes such as snow accumulation. The latter is challenging to observe on a continental scale and in situ data are sparse, so we largely rely on estimates from atmospheric models. Here, we employ a novel method, GPS interferometric reflectometry (GPS-IR), to measure upper (<2 m) firn-column thickness changes across a 23-station GPS array in West Antarctica. We compare the results with antenna heights measured in situ to establish the method's daily uncertainty (0.06 m) and with output from two atmospheric reanalysis products to categorize spatial and temporal variability of net snow accumulation. GPS-IR is an effective method for monitoring surface mass-balance processes that can be applied to both historic GPS datasets and future experiments to provide critical in situ observations of processes driving surface-height evolution.

Keypoints:

- We apply a method established in Greenland to measure Antarctic snow accumulation at daily resolution from GPS data.

[5]Earth and Planetary Sciences, University of California, Santa Cruz, Santa Cruz, CA, USA.

- We compare results from a 23-station array with in situ data and surface fields from two state-of-the-art atmospheric reanalysis products.
- We suggest that historic ice-sheet GPS records could be revisited and that future research should be designed considering this application

1. Introduction

Ice-sheet mass-balance, and an ice sheet's ultimate contribution to global sea-level change, is controlled by mass gain through snowfall and mass loss through ice flux to the ocean, sublimation, and surface-melt runoff, the latter of which is negligible for most of the Antarctic ice sheet. While ice discharge can be estimated on regional- to continental-scales with remote sensing techniques [e.g., *Rignot et al.*, 2013], net snow accumulation—the balance between snowfall and sublimation—in Antarctica is both harder to constrain and more variable in time and space. In particular, observational records of snow accumulation typically only sample one dimension: ice and firn cores sample a single location with typically annual resolution [e.g., *Kaspari et al.*, 2004], while accumulation stake forests capture spatial variability over short time intervals [e.g., *Frezzotti et al.*, 2005]. More recently, methods using airborne radar to derive multi-decadal records of annual accumulation have been developed [*Medley et al.*, 2013], but are limited in spatial coverage.

Since the Antarctic ice sheet is so large, there are only sparse in situ snow accumulation observations, and continental-scale Antarctic ice-sheet mass balance estimates [e.g., *Shepherd et al.*, 2012] must instead use global reanalysis products or regional climate models, the latter being forced by the former. These products are generated by assimilating remotely sensed and point-based observations with models of atmospheric physics to recreate past atmospheric states, outputting atmospheric parameters that are discretized in space and time, which are then used to derive ice-sheet surface mass balance. While the spatial pattern of accumulation from various models has been evaluated with in situ data [e.g. *van de Berg et al.*, 2006; *Lenaerts et al.*, 2012b; *Wessem et al.*, 2014], difficulty

remains in assessing their temporal behavior, especially at sub-annual resolution [*Eisen et al.*, 2008]. Sonic rangers associated with automatic weather stations are a potential mechanism for validating accumulation products at periods of one year or shorter, but spatial resolution issues (i.e., point measurements versus grid resolutions of several 10s of km) limit effective comparison.

In this paper, we investigate an alternative technique for acquiring information about surface processes: the reflected signal from Global Positioning System (GPS) satellites, or GPS interferometric reflectometry (GPS-IR). Multiple studies have shown that this reflected signal contains information about the surface surrounding a GPS station, including soil moisture [e.g., *Larson et al.*, 2008a], snow depth [e.g., *Larson et al.*, 2009], and firn compaction in Greenland [e.g., *Larson et al.*, 2015]. We demonstrate the utility of GPS-IR for generating precise time series of time-integrated snow accumulation in Antarctica (i.e., the difference between snowfall and sublimation), by comparing surface-height changes derived from GPS-IR to in situ measurements and two atmospheric reanalysis products.

2. Data and Methods

2.1. GPS Data Collection and Processing

2.1.1. Field Site

The lower confluence of Mercer and Whillans ice streams have been instrumented with an array of up to 23 continuous GPS instruments between 2007 and 2016 (Figure 1). Each station consists of a Trimble NetRS or NetR9 receiver, a Trimble Zephyr Geodetic or Zephyr Geodetic II antenna mounted on a 3–4 m metal pole installed 1–2 m into

the surface, and a power bank (1–2 solar panels, 0–2 wind turbines, 4–10 batteries). This GPS experiment has spanned multiple projects with different geophysical goals, including investigation of ice dynamics, subglacial hydrology, and ice-ocean interaction [*Beem et al.*, 2014; *Siegfried et al.*, 2014, 2016; *Fricker et al.*, 2015; *Siegfried*, 2015; *Marsh et al.*, 2016], driving changes to the array geometry over the past decade and resulting in 42 distinct locations occupied since 2010. Each austral summer between December 2011 and December 2016, we measured antenna heights (h_{meas}) by hand across the array, for a total of 114 observations. Although our GPS array was not designed for investigating ice-sheet surface processes, it provides an unprecedented, regional, long-term dataset to demonstrate the potential of GPS-IR to study snow accumulation (and likely other surface processes).

2.1.2. GPS-IR

Conventional GPS positioning uses coded signals transmitted by the GPS satellite constellation at two L-band frequencies (L1 at 1575.42 MHz; L2 at 1226.60 MHz) to derive a three-dimensional position estimate of antenna location [*Bock and Melgar*, 2016]. Accuracy of position estimates are reduced when indirect, reflected signals interfere with the direct signal at the GPS receiver antenna. Although this "multipath" signal is conventionally treated as noise, it contains useful information about the reflection surface (or surfaces); GPS-IR analyses isolate this signal [e.g., *Larson et al.*, 2008b]. Our GPS-IR processing strategy follows that of *Larson et al.* [2015], who used GPS-IR to estimate firn compaction rates at three sites on the Greenland ice sheet.

The basic principle behind GPS-IR over ice sheets is that the signal reflected from the snow surface has a longer path-length than the signal that travels directly between the GPS satellite antenna and the GPS receiver antenna (Figure 2a). The two signals interfere at the antenna, and the strength of the resulting signal (recorded by the GPS receiver as the signal-to-noise ratio, or SNR) varies as a function of GPS satellite elevation angle (Figure 2b). The frequency of this SNR interference pattern depends on the ratio between the reflector height (i.e., the vertical distance between the snow surface and the phase center of the GPS receiver antenna) and the GPS signal wavelength. Similar to *Larson et al.* [2015], we opt to use the civilian code on the L1 frequency (i.e., L1 Coarse Acquisition, or C/A) rather than on the L2 frequency (i.e., L2C) as L2C is currently only transmitted by a subset of satellites in the constellation whereas L1 is available for all 30+ satellites for the duration of our experiment.

Due to the GPS antenna gain pattern, which was designed to suppress multipath signals, interference between direct and reflected signals can only be seen at low satellite-elevation angles, i.e. when the satellite is rising or setting. Therefore, we first filter to exclude data acquired when the satellite elevation angle was greater than 25°. We then remove the background trend of SNR increase with satellite-elevation angle using a third-order polynomial fit (Figure 2b) and estimate a reflector height by determining the dominant frequency of L1 C/A SNR modulation with a Lomb-Scargle periodogram [*Press et al.*, 1996] (Figure 2c). We correct the reflector height for the distance between antenna phase center and antenna base; the resulting height estimate represents the mean antenna height above the snow surface over the sensing footprint, which is an ellipse ∼4 m wide extending

up to ∼34 m (or 2× the distance to the reflection point) for a 2 m high antenna from the receiver antenna in the direction of the GPS satellite.

We estimate a daily averaged antenna height over the snow surface (h_{gps-ir}) by calculating the median reflector height for all rising and setting satellites over 24 hours. Therefore, for a 2 m high GPS antenna, the footprint is a circle of radius ∼34 m surrounding the antenna, or ∼3600 m^2 (Figure 2d). The area covered by GPS-IR can be tuned by changing the height of the GPS antenna.

Previous work has combined estimates of h_{gps-ir} with conventional GPS position techniques to estimate rates of firn compaction [e.g., *Larson et al.*, 2015]. We seek to retrieve the time evolution of surface height, so we calculate the reflector height at t_0 (determined as the mean of the first month of data) and our daily reflector height values $h_{gps-ir}(t)$. The difference between these two ($\Delta h_{surf}(t) = h_{gps-ir}(t_0) - h_{gps-ir}(t)$) represents the change in thickness of the firn column between the surface and the anchor point of the GPS antenna installation (typically 1–2 m below the surface) and is not sensitive to processes occurring below this horizon, such as height change due to firn compaction below the anchor point, ice dynamics, basal topography, or glacial isostatic adjustment.

$\Delta h_{surf}(t)$ is sensitive to five near-surface processes:

$$\Delta h_{surf}(t) = P(t) - M(t) - E(t) + h_w(t) + h_{fc}^{z=0\sim2}(t) \quad (1)$$

where $P(t)$ is precipitation in meters of snow, $M(t)$ is surface melt, $E(t)$ is evaporation and sublimation, $h_w(t)$ is height change due to wind redistribution of surface snow, and $h_{fc}^{z=0\sim2}(t)$ is height change due to firn compaction occurring from $z = 0$ m to to $z = \sim2$ m of the column. Because surface melt is negligible in Antarctica, the observation integrates

over a large enough area to minimize noise from small-scale wind-induced variability, and the integrated compaction of the top 1–2 m is relatively small even though it is the firn that undergoes the most rapid compaction, $\Delta h_{surf}(t)$ largely represents surface accumulation $(P(t) - E(t))$.

2.2. Atmospheric Reanalysis Products

We use two different atmospheric reanalysis products: the European Centre for Medium-Range Weather Forecasts' ERA-Interim [*Dee et al.*, 2011] and NASA's Modern-Era Retrospective analysis for Research and Applications, Version 2 (MERRA-2) [*Gelaro et al.*, 2017] (see *Fujiwara et al.* [2017] for a comparison of the relative strengths of these products). Because our GPS-IR method isolates changes in thickness of the upper 1–2 m of the firn column, we are only interested in two reanalysis parameters: total precipitation and evaporation (which includes sublimation). We estimate daily values of $P(t) - E(t)$ at each GPS location to approximate the net accumulation for each reanalysis product and integrate these daily values through time to generate a time series of height change. Initially, we generate the accumulation products in meters of water equivalent, which need to be scaled by the surface snow density (ρ_{snow}) to estimate a true surface-height change that is comparable to GPS-IR results. We perform this scaling in two ways: (1) by assuming a range of ρ_{snow} between 250 and 350 kg m^{-3}; and (2) by minimizing the misfit between the slopes of GPS-IR- and reanalysis-derived integrated accumulation.

3. Results and Discussion

3.1. GPS-IR Validation

We compare GPS-IR-derived antenna heights with 114 coincident observations of antenna height measured in the field between Dec. 2011 and Dec. 2016 (Figure 3). The mean difference between GPS-IR and measured antenna heights is 0.02 ± 0.06 m (1σ). GPS-IR overestimates antenna height (though by less than previously estimated in the western United States [*Larson and Small*, 2016]), which could be due to several factors: penetration of the L-band GPS signal into near-surface snow (estimated to be 0.01–0.02 m for L1 at low incident angles [*Nievinski*, 2013]), reflection shadows caused by surface roughness, or drifting snow near the antenna pole (biasing in situ measurements). Because one major strength of our GPS-IR method is the ability to generate high-resolution time series of surface-height change, a small bias in retrieved antenna height is not problematic as long as the measurement is robust, i.e. the magnitude of the bias does not change through time. From our 114 in situ estimates acquired over five years, the bias does not vary interannually; we cannot assess any seasonal bias as we only have in situ measurements during austral summer.

The cm-scale variability in the difference between measured and estimated antenna height results from uncertainty in the GPS-IR method, uncertainty in the field measurement, and nonlinear surface topography within the sensing footprint (i.e., height at the antenna is not the arithmetic mean of topography within the footprint). We estimate uncertainty of our field measurements to be 0.01–0.02 m (due to estimating where the "true" snow surface relative to the disturbed surface), suggesting the majority of imprecision is a result of GPS-IR processing uncertainty and small amplitude topography within

the sensing footprint. Future work combining L1 C/A height estimates with analysis of reflected signals from the GPS L2C band as well as from other satellite navigation systems (e.g., GLONASS, Galileo, BeiDou) may be able to improve GPS-IR precision.

3.2. Surface Evolution from GPS-IR

For each of the 42 continuous GPS locations, we generated a time series of $\Delta h_{surf}(t)$ ranging from 1 to 7 years, comprising 29,653 independent daily height retrievals. We analyzed subsets of the array to highlight the capability of our method for investigating temporal and spatial variability of net accumulation. Four GPS stations (Figure 1, blue circles) have seven years of nearly uninterrupted daily resolution: LA09 (2008–2015), LA02, LA07, and LA08 (2010–2017). These stations all show a positive $\Delta h_{surf}(t)$ trend (Figure 4a-d), with rates of 0.164 m yr^{-1}, 0.213 m yr^{-1}, 0.215 m yr^{-1}, and 0.169 m y^{-1} for LA02, LA07, LA08, and LA09, respectfully. Because we have not included a correction for firn compaction, our results are likely an underestimate by 0.03–0.04 m yr^{-1}, based on *Herron and Langway* [1980].

These accumulate rates compare favorably with the mean rate of 0.22 m yr^{-1} over a 42-year period (1955–1997) derived from two shallow (< 20 m) ice cores near the northern shear margin of Whillans Ice Stream [*Spikes et al.*, 2003] and a rate of $\sim$0.25 m yr^{-1} from snow pit measurements further upstream [*Alley and Bentley*, 1988], yet the new measurements show persistent spatial variability of up 25% over distances <40 km. Therefore, we cannot assess whether the difference between previous observations of snow accumulation and our GPS-IR derived estimates is due to a decadal-scale secular decrease in accumulation rate or inherent differences between the six different sites. Our GPS-IR

observations also reveal interannual variability of 0.05–0.10 m yr^{-1}, comparable to the 0.05–0.06 m yr^{-1} estimated by *Alley and Bentley* [1988], *Venteris and Whilans* [1998], and *Spikes et al.* [2003], as well as larger deviations, such as the nearly 0.20 m negative anomaly during the 2010–2011 austral summer seen at LA07, LA08, and LA09 (Figure S1).

Results from a transect of GPS stations across the grounding line (Figure 1, red circles), where the ice sheet transitions from fully grounded on land to fully floating on ocean, illustrate the potential of GPS-IR to quantify spatial variability of accumulation, as well as other surface processes, on kilometer scales. Stations GZ01 to GZ05 were oriented perpendicular to the grounding line, were spaced at approximately 6 km, and were operated for three years (2011–2014; Figure 5). Mean annual snow accumulation during this three year period varies by nearly 200% across this 24 km transect, with a height-change rate of 0.432 m yr^{-1} at GZ01 (fully grounded), decreasing to 0.222 m yr^{-1} at GZ05 (fully floating). This trend corresponds to small topographic gradients across the transect, with a slope of -0.03° from GZ01 to GZ03 (-6.40 m over 11.73 km) and a slope of +0.003° from GZ03 to GZ05 (0.70 m over 11.76 km).

3.3. Comparison between GPS-IR and Reanalysis Products

For the four GPS sites with seven years of data, we compare GPS-IR $\Delta h_{surf}(t)$ to ERA-Interim and MERRA-2 $P(t)-E(t)$ by scaling reanalysis products with an optimized ρ_{snow} (Figure 4a-d). We then can use this best-fit ρ_{snow} as a diagnostic tool for assessing potential biases in reanalysis $P(t)-E(t)$ by comparing its value to the few in situ studies of near-surface snow density on or near Whillans Ice Stream, which range from 300 to

370 kg m^{-3} [*Alley and Bentley*, 1988; *Retzlaff and Bentley*, 1993; *Venteris and Whilans*, 1998; *Spikes et al.*, 2003; *Picotti et al.*, 2015]. Modeled surface densities for the Whillans Ice Stream region lie slightly above the observed range, at 360–400 kg m^{-3} [*Ligtenberg et al.*, 2011].

ERA-Interim ρ_{snow} are consistently lower than that for MERRA-2, ranging from 35% to 74% of the MERRA-2 value, and fall below both the observed and modeled values for the region, indicating that ERA-Interim is underestimating net accumulation. MERRA-2 densities are similar to surface densities modeled for the region, though are above the observed values, suggesting MERRA-2 might be overestimating net accumulation. There is a general trend from both ERA-Interim and MERRA-2 of increasing snow density along flow on the LA09-LA08-LA07 flow line (Figure 4a-c), which could reflect a real change in surface conditions (e.g., a change in mean wind velocity driving changes in density of precipitating snow [*Meløysund et al.*, 2007]) or potential biases in the reanalysis products that are compensated by increasing ρ_{snow} to match observations (e.g., the reanalysis products overestimate precipitation at lower elevations as there are 20 m differences in elevation between these sites). Without additional data, trends in the optimized ρ_{snow} are hard to attribute; simple purpose-designed experiments combining GPS-IR with shallow snow pits and anemometers can drive detailed studies to separate biases in reanalysis products from true spatial trends in surface conditions. Best-fitting ρ_{snow} values for ERA-Interim and MERRA-2 at LA02 (Figure 4d) have the largest difference from each other and from observed values. This site is on a subglacial lake defined by a 10–15 km wide, ∼15 m deep surface depression [*Christianson et al.*, 2012], suggesting that the spatial resolution

at which reanalysis products are generated cannot fully capture the observed pattern because neither small-scale topography nor wind redistrubition is represented.

Power spectral densities of the residuals between reanalysis and GPS-IR data (Figure 4e-h) show that, while both reanalysis products effectively capture sub-annual variability, neither reanalysis product captures the multiyear variability seen in observations. ERA-Interim also overestimates the annual signal in net accumulation, which further analysis suggests is a result of biased snow accumulation rather than sublimation. While GPS-IR's spatial footprint is notably larger than previous ground-based point measurements, there is still a significant mismatch in scale between GPS-IR (1000s of m^2) and reanalysis products (100s of km^2), which impacts our comparisons.

Neither ERA-Interim nor MERRA-2 capture the 200% variability in accumulation along the GZ01-GZ05 transect (Figure 5), which is likely related to a combination of the coarse resolution of both products ($0.625° \times 0.5°$ [69 km × 5.8 km at 84°S] for MERRA-2; $0.75° \times 0.75°$ [83 km × 8.7 km at 84°S] for ERA-Interim) and wind redistribution of snow after deposition. Although ERA-Interim again underestimates net accumulation by ∼50%, this reanalysis product does show a minor trend of lower accumulation along the grounded-to-floating transect. MERRA-2 has a larger spread in accumulation along the transect, but the value is lowest at the fully grounded size (GZ01), contrary to the observations. This section of the grounding line is complex: the transect is perpendicular to the grounding line and oblique to both ice flow and dominate wind direction, and is located on the flank of a narrow grounding line embayment characterized by low slopes (compared to other grounding lines [e.g., *Horgan and Anandakrishnan*, 2006]). While a

quantitative investigation of the drivers short-scale spatial variability at this site requires additional datasets and a different GPS array geometry, the substantial sub-grid scale variability we observe highlights the difficulty in evaluating the performance of surface-process models in Antarctic: capturing variability in complex, but critical regions like grounding lines will require higher resolution or adaptive mesh models to resolve the important feedbacks between topography, precipitation, wind, and drifting snow [e.g., *Lenaerts et al.*, 2012a]. GPS-IR experiments designed specifically for surface process investigation can provide valuable datasets for observing these processes and validating models as they are improved.

4. Summary

We applied GPS-IR methods at 42 stations across the Whillans and Mercer ice streams, West Antarctica, to retrieve estimates of net snow accumulation, and validated the retrievals with in situ field measurements. We demonstrated that GPS-IR surface-height estimates in the region are accurate to 0.02 m and precise to 0.06 m. We then used our GPS-IR observations to investigate spatial and temporal variability in snow accumulation at our study site and compared our results to past results and two widely used atmospheric reanalysis products. Our GPS-IR observations indicated that both reanalysis products effectively capture sub-annual structure of accumulation, but both have persistent absolute biases and are likely underestimating interannual variability.

The success of the GPS-IR technique and the relative ease of GPS deployments (in terms of both cost and logistics) imply that future experiments can be readily developed and executed to isolate individual processes that have been difficult or prohibitively expensive

to previously assess with field measurements, such as wind scour and deposition, firn compaction, and time-variability of volume scattering of satellite radar altimeters. While our study site consists of a simple geometry for the GPS-IR method (i.e., flat), it is representative of a large portion of Antarctica, especially the East Antarctic plateau, where cm-level precision of surface height is required for robust ice-sheet mass-balance estimates.

This study is the first attempt at a detailed in situ validation of GPS-IR surface-height change measurements on an ice sheet, with only one previous qualitative comparison of this type was performed with an ultrasonic snow logger at a single location in Greenland, but no quantitative results were given [*Larson et al.*, 2015]. Our results demonstrate that GPS-IR is an effective method for determining surface-height change over the Antarctic ice sheet at daily resolution with cm-level precision, that can yield unique and significant insights into ice-sheet surface processes. This implies that historic GPS records acquired over the past two decades from Greenland and Antarctica could be revisited, and future experiments should be designed with this application in mind.

Acknowledgments. GPS data collection and analysis was supported by NSF grants to H.A.F. (ANT-0838885, ANT-1543441) and S.T. (ANT-0636970, ANT-0838947, ANT-0839142) as part of the interdisciplinary WISSARD and SALSA projects. Method development was supported by an NSF grant to K.M.L. (AGS-1449554). M.R.S. was supported in by part the George Thompson Fellowship at Stanford University. We thank the 2010–2017 WISSARD and SALSA field team members for data collection assistance and UNAVCO, Raytheon Polar Services, Antarctic Support Contract, Kenn Borek Air, and

the New York Air National Guard for logistical support. Data used in this manuscript are available by contacting the corresponding author directly.

References

Alley, R. B., and C. R. Bentley (1988), Ice-Core Analysis on the Siple Coast of West Antarctica, *Annals of Glaciology*, *11*, 1–7, doi:10.1017/s0260305500006236.

Beem, L. H., S. M. Tulaczyk, M. A. King, M. Bougamont, H. A. Fricker, and P. Christoffersen (2014), Variable deceleration of Whillans Ice Stream, West Antarctica, *Journal of Geophysical Research: Earth Surface*, *119*(2), 212–224.

Bock, Y., and D. Melgar (2016), Physical applications of GPS geodesy: a review, *Reports on Progress in Physics*, *79*(10), 106,801, doi:10.1088/0034-4885/79/10/106801.

Christianson, K., R. W. Jacobel, H. J. Horgan, S. Anandakrishnan, and R. B. Alley (2012), Subglacial Lake Whillans — Ice-penetrating radar and GPS observations of a shallow active reservoir beneath a West Antarctic ice stream, *Earth and Planetary Science Letters*, *331-332*, 237–245, doi:10.1016/j.epsl.2012.03.013.

Dee, D. P., S. M. Uppala, A. J. Simmons, P. Berrisford, P. Poli, S. Kobayashi, U. Andrae, M. A. Balmaseda, G. Balsamo, P. Bauer, P. Bechtold, A. C. M. Beljaars, L. van de Berg, J. Bidlot, N. Bormann, C. Delsol, R. Dragani, M. Fuentes, A. J. Geer, L. Haimberger, S. B. Healy, H. Hersbach, E. V. Hólm, L. Isaksen, P. Kållberg, M. Köhler, M. Matricardi, A. P. McNally, B. M. Monge-Sanz, J.-J. Morcrette, B.-K. Park, C. Peubey, P. de Rosnay, C. Tavolato, J.-N. Thépaut, and F. Vitart (2011), The ERA-Interim reanalysis: configuration and performance of the data assimilation system, *Quarterly Journal of the Royal Meteorological Society*, *137*(656), 553–597, doi:10.1002/qj.828.

Depoorter, M. A., J. L. Bamber, J. A. Griggs, J. T. M. Lenaerts, S. R. M. Ligtenberg, M. R. van den Broeke, and G. Moholdt (2013), Calving fluxes and basal melt rates of Antarctic ice shelves, *Nature*, *502*(7469), 89–92, doi:10.1038/nature12567.

Eisen, O., M. Frezzotti, C. Genthon, E. Isaksson, O. Magand, M. R. van den Broeke, D. A. Dixon, A. Ekaykin, P. Holmlund, T. Kameda, L. Karlöf, S. Kaspari, V. Y. Lipenkov, H. Oerter, S. Takahashi, and D. G. Vaughan (2008), Ground-based measurements of spatial and temporal variability of snow accumulation in east antarctica, *Reviews of Geophysics*, *46*(2), doi:10.1029/2006rg000218.

Frezzotti, M., M. Pourchet, O. Flora, S. Gandolfi, M. Gay, S. Urbini, C. Vincent, S. Becagli, R. Gragnani, M. Proposito, M. Severi, R. Traversi, R. Udisti, and M. Fily (2005), Spatial and temporal variability of snow accumulation in East Antarctica from traverse data, *Journal of Glaciology*, *51*(172), 113–124, doi:10.3189/172756505781829502.

Fricker, H. A., M. R. Siegfried, S. P. Carter, and T. A. Scambos (2015), A decade of progress in observing and modeling Antarctic subglacial water systems, *Philosophical Transactions of the Royal Society A*, *374*(2059), 20140,294, doi:10.1098/rsta.2014.0294.

Fujiwara, M., J. S. Wright, G. L. Manney, L. J. Gray, J. Anstey, T. Birner, S. Davis, E. P. Gerber, V. L. Harvey, M. I. Hegglin, et al. (2017), Introduction to the sparc reanalysis intercomparison project (s-rip) and overview of the reanalysis systems, *Atmospheric Chemistry and Physics*, *17*(2), 1417–1452.

Gelaro, R., W. McCarty, M. J. Suárez, R. Todling, A. Molod, L. Takacs, C. Randles, A. Darmenov, M. G. Bosilovich, R. Reichle, et al. (2017), The Modern-Era Retrospective

Analysis for Research and Applications, Version 2 (MERRA-2), *Journal of Climate*, (2017).

Herron, M. M., and C. C. Langway (1980), Firn densification: an empirical model, *Journal of Glaciology*, *25*(93), 373–385.

Horgan, H. J., and S. Anandakrishnan (2006), Static grounding lines and dynamic ice streams: Evidence from the Siple Coast, West Antarctica, *Geophysical Research Letters*, *33*(18), n/a–n/a, doi:10.1029/2006gl027091.

Kaspari, S., P. A. Mayewski, D. A. Dixon, V. B. Spikes, S. B. Sneed, M. J. Handley, and G. S. Hamilton (2004), Climate variability in West Antarctica derived from annual accumulation-rate records from ITASE firn/ice cores, *Annals of Glaciology*, *39*(1), 585–594, doi:10.3189/172756404781814447.

Larson, K. M., and E. E. Small (2016), Estimation of Snow Depth Using L1 GPS Signal-to-Noise Ratio Data, *IEEE Journal of Selected Topics in Applied Earth Observations and Remote Sensing*, *9*(10), 4802–4808, doi:10.1109/jstars.2015.2508673.

Larson, K. M., E. E. Small, E. D. Gutmann, A. L. Bilich, J. J. Braun, and V. U. Zavorotny (2008a), Use of GPS receivers as a soil moisture network for water cycle studies, *Geophysical Research Letters*, *35*(24), doi:10.1029/2008gl036013.

Larson, K. M., E. E. Small, E. Gutmann, A. Bilich, P. Axelrad, and J. Braun (2008b), Using GPS multipath to measure soil moisture fluctuations: initial results, *GPS Solutions*, *12*(3), 173–177, doi:10.1007/s10291-007-0076-6.

Larson, K. M., E. D. Gutmann, V. U. Zavorotny, J. J. Braun, M. W. Williams, and F. G. Nievinski (2009), Can we measure snow depth with GPS receivers?, *Geophysical*

Research Letters, *36*(17), doi:10.1029/2009gl039430.

Larson, K. M., J. Wahr, and P. K. Munneke (2015), Constraints on snow accumulation and firn density in Greenland using GPS receivers, *Journal of Glaciology*, *61*(225), 101–114, doi:10.3189/2015jog14j130.

Lenaerts, J. T., M. R. V. D. Broeke, C. Scarchilli, and C. Agosta (2012a), Impact of model resolution on simulated wind, drifting snow and surface mass balance in Terre Adélie, East Antarctica, *Journal of Glaciology*, *58*(211), 821–829, doi:10.3189/2012jog12j020.

Lenaerts, J. T. M., M. R. van den Broeke, W. J. van de Berg, E. van Meijgaard, and P. K. Munneke (2012b), A new, high-resolution surface mass balance map of Antarctica (1979-2010) based on regional atmospheric climate modeling, *Geophysical Research Letters*, *39*(4), n/a–n/a, doi:10.1029/2011gl050713.

Ligtenberg, S. R. M., M. M. Helsen, and M. R. van den Broeke (2011), An improved semi-empirical model for the densification of Antarctic firn, *The Cryosphere*, *5*(4), 809–819, doi:10.5194/tc-5-809-2011.

Marsh, O. J., H. A. Fricker, M. R. Siegfried, K. Christianson, K. W. Nicholls, H. F. J. Corr, and G. Catania (2016), High basal melting forming a channel at the grounding line of Ross Ice Shelf, Antarctica, *Geophysical Research Letters*, *43*(1), 250–255, doi:10.1002/2015gl066612.

Medley, B., I. Joughin, S. B. Das, E. J. Steig, H. Conway, S. Gogineni, A. S. Criscitiello, J. R. McConnell, B. E. Smith, M. R. van den Broeke, J. T. M. Lenaerts, D. H. Bromwich, and J. P. Nicolas (2013), Airborne-radar and ice-core observations of annual snow accumulation over Thwaites Glacier, West Antarctica confirm the spatiotempo-

ral variability of global and regional atmospheric models, *Geophysical Research Letters*, *40*(14), 3649–3654, doi:10.1002/grl.50706.

Meløysund, V., B. Leira, K. V. Høiseth, and K. R. Lisø (2007), Predicting snow density using meteorological data, *Meteorological Applications*, *14*(4), 413–423, doi:10.1002/met.40.

Nievinski, F. G. (2013), Forward and Inverse Modeling of GPS Multipath for Snow Monitoring, Ph.D. thesis, University of Colorado.

Picotti, S., A. Vuan, J. M. Carcione, H. J. Horgan, and S. Anandakrishnan (2015), Anisotropy and crystalline fabric of Whillans Ice Stream (West Antarctica) inferred from multicomponent seismic data, *Journal of Geophysical Research: Solid Earth*, *120*(6), 4237–4262, doi:10.1002/2014jb011591.

Press, W., S. A. Teukolski, W. T. Vetterling, and B. P. Flannery (1996), *Numerical Recipes in Fortran 90: The Art of Parallel Scientific Computing*, Cambridge University Press, Cambridge England New York.

Retzlaff, R., and C. R. Bentley (1993), Timing of stagnation of Ice Stream C, West Antarctica, from short-pulse radar studies of buried surface crevasses, *Journal of Glaciology*, *39*, 553–561.

Rignot, E., S. Jacobs, J. Mouginot, and B. Scheuchl (2013), Ice-Shelf Melting Around Antarctica, *Science*, *341*(6143), 266–270, doi:10.1126/science.1235798.

Scambos, T. A., T. M. Haran, M. A. Fahnestock, T. H. Painter, and J. Bohlander (2007), MODIS-based Mosaic of Antarctica (MOA) data sets: Continent-wide surface morphology and snow grain size, *Remote Sensing of Environment*, *111*(2), 242–257.

Shepherd, A., E. R. Ivins, G. A, V. R. Barletta, M. J. Bentley, S. Bettadpur, K. H. Briggs, D. H. Bromwich, R. Forsberg, N. Galin, M. Horwath, S. Jacobs, I. Joughin, M. A. King, J. T. M. Lenaerts, J. Li, S. R. M. Ligtenberg, A. Luckman, S. B. Luthcke, M. McMillan, R. Meister, G. Milne, J. Mouginot, A. Muir, J. P. Nicolas, J. Paden, A. J. Payne, H. Pritchard, E. Rignot, H. Rott, L. S. Sorensen, T. A. Scambos, B. Scheuchl, E. J. O. Schrama, B. Smith, A. V. Sundal, J. H. van Angelen, W. J. van de Berg, M. R. van den Broeke, D. G. Vaughan, I. Velicogna, J. Wahr, P. L. Whitehouse, D. J. Wingham, D. Yi, D. Young, and H. J. Zwally (2012), A Reconciled Estimate of Ice-Sheet Mass Balance, *Science*, *338*(6111), 1183–1189, doi:10.1126/science.1228102.

Siegfried, M. R. (2015), Investigating Antarctic ice sheet subglacial processes beneath the Whillans Ice Plain, West Antarctica, using satellite altimetry and GPS, Ph.D. thesis, University of California, San Diego.

Siegfried, M. R., H. A. Fricker, M. Roberts, T. A. Scambos, and S. Tulaczyk (2014), A decade of West Antarctic subglacial lake interactions from combined ICESat and CryoSat-2 altimetry, *Geophysical Research Letters*, *41*(3), 891–898, doi:10.1002/2013GL058616.

Siegfried, M. R., H. A. Fricker, S. P. Carter, and S. Tulaczyk (2016), Episodic ice velocity fluctuations triggered by a subglacial flood in West Antarctica, *Geophysical Research Letters*, *43*(6), 2640–2648, doi:10.1002/2016GL067758.

Spikes, V. B., B. M. Csathó, G. S. Hamilton, and I. M. Whillans (2003), Thickness changes on Whillans Ice Stream and Ice Stream C, West Antarctica, derived from laser altimeter measurements, *Journal of Glaciology*, *49*(165), 223–230, doi:

10.3189/172756503781830683.

van de Berg, W. J., M. R. van den Broeke, C. H. Reijmer, and E. van Meijgaard (2006), Reassessment of the Antarctic surface mass balance using calibrated output of a regional atmospheric climate model, *Journal of Geophysical Research*, *111*(D11), doi: 10.1029/2005jd006495.

Venteris, E. R., and I. M. Whilans (1998), Variability of accumulation rate in the catchments of Ice Streams B, C, D and E, Antarctica, *Annals of Glaciology*, *27*(1), 227–230.

Wessem, J. V., C. Reijmer, M. Morlighem, J. Mouginot, E. Rignot, B. Medley, I. Joughin, B. Wouters, M. Depoorter, J. Bamber, J. Lenaerts, W. D. V. Berg, M. V. D. Broeke, and E. V. Meijgaard (2014), Improved representation of East Antarctic surface mass balance in a regional atmospheric climate model, *Journal of Glaciology*, *60*(222), 761–770, doi:10.3189/2014jog14j051.

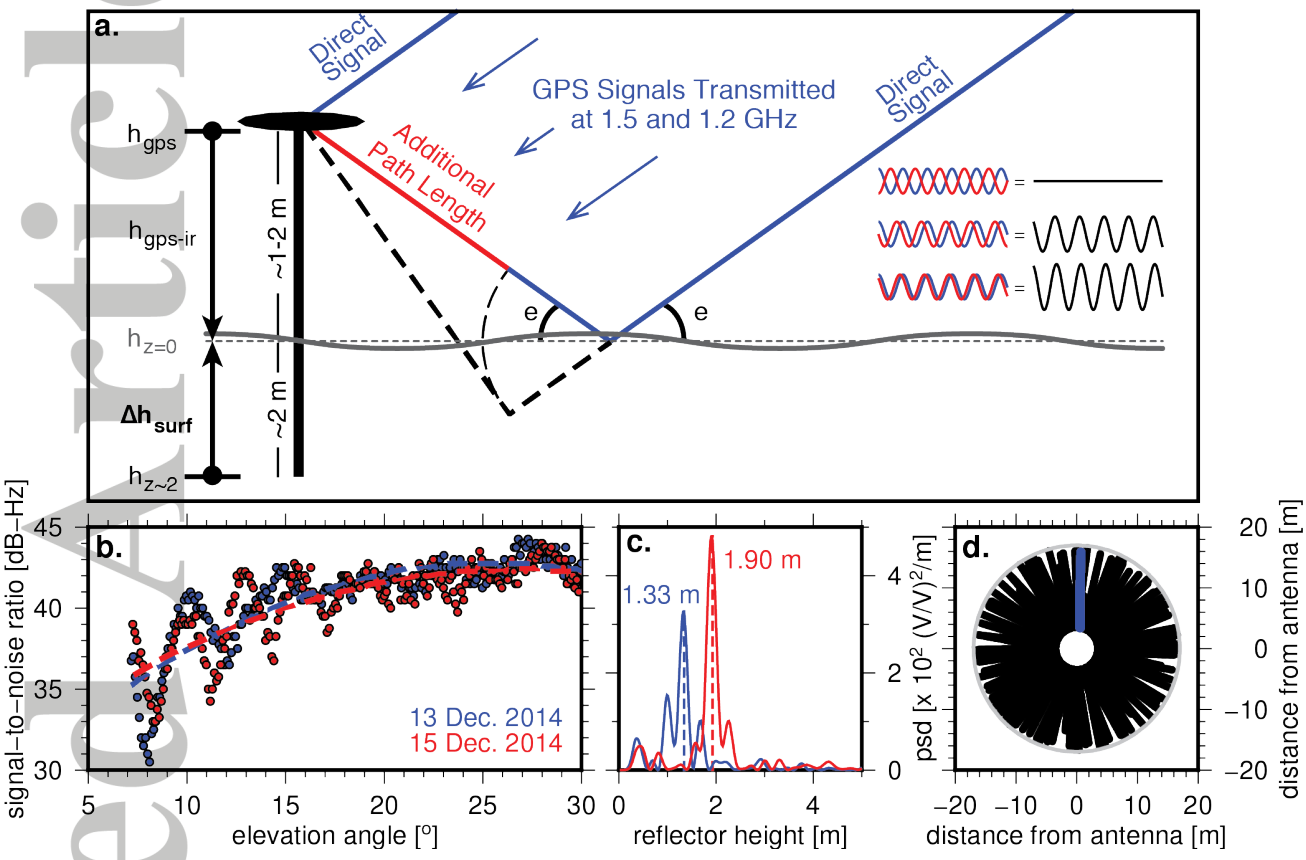

Figure 1. Map showing the locations of our continuous GPS sites on the lower confluence of Mercer and Whillans ice streams, West Antarctica. Black circles correspond to locations of all GPS stations since 2010. Blue filled circles are GPS sites shown in Figure 4. Red filled circles are GPS sites shown in Figure 5. Background imagery from MODIS Mosaic of Antarctica [*Scambos et al.*, 2007]; grounding line from a multi-technique synthesis by *Depoorter et al.* [2013].

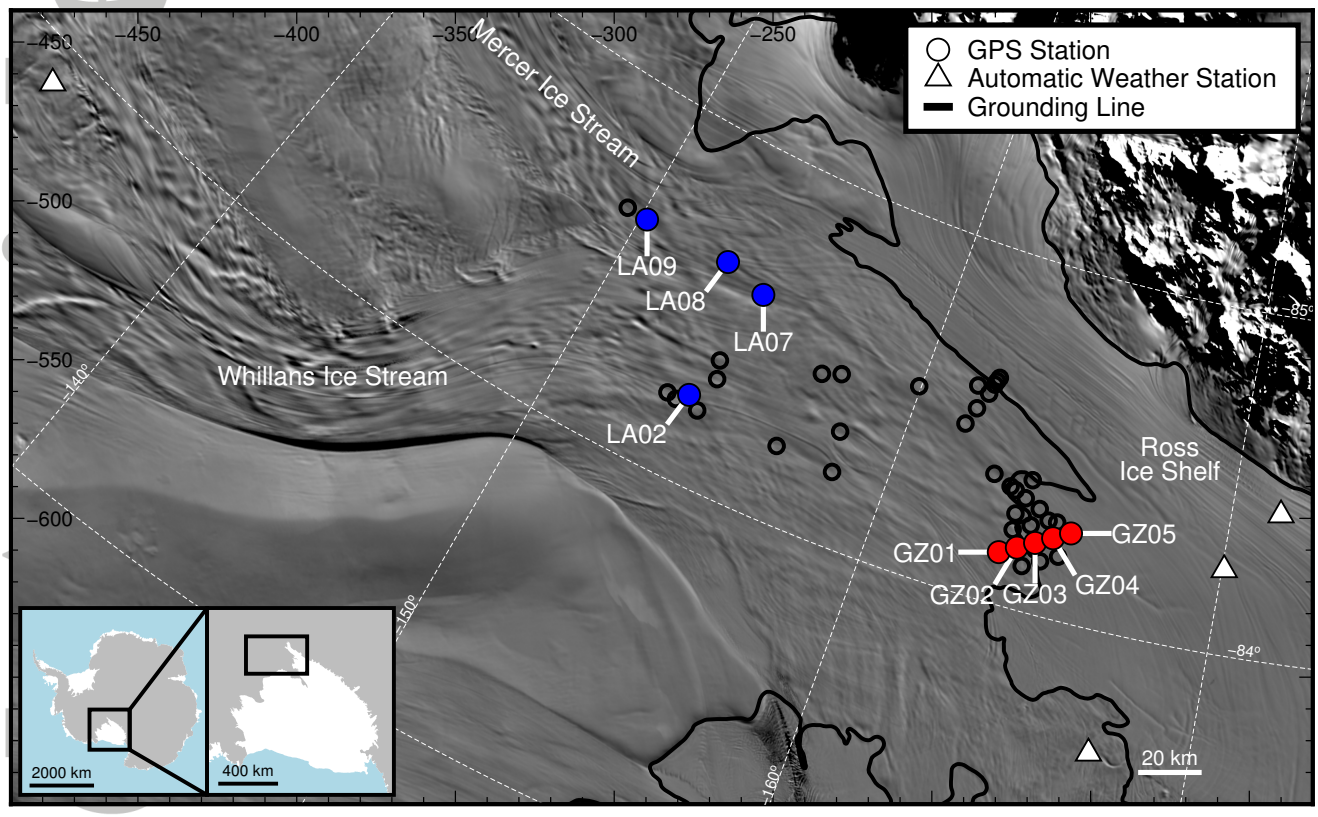

Figure 2. (a) Schematic of GPS-IR (after *Larson et al.* [2015]) showing experiment setup and basis for our method. GPS receiver antenna is mounted on a pole 1–2 m above the snow surface, with the pole anchored ∼2 m below the surface. Some of the transmitted signal from a GPS satellite at elevation angle e arrive at the antenna directly (blue) and some reflect off the snow surface before arriving at the GPS antenna (red), increasing the path length. Inset: The direct and reflected signal interfere to produce the recorded signal-to-noise ratio (SNR) observation (black). (b) Example of recorded SNR as a function of satellite elevation angle at LA09 for one rising satellite on 13 Dec. 2014 and 15 Dec. 2014; antenna was raised by hand on 14 Dec. 2014 by 0.52 m based on in situ measurements. (c) Power spectral density of SNR for the rising satellite shown in (b), where peak amplitude corresponds to the reflector height estimate (not yet corrected for antenna phase center offset). (d) Map of GPS reflection points surrounding a 2 m high GPS antenna (positioned at 0,0) for the rising satellite on 13 Dec. 2014 (blue) and the full day (black). Radius of gray circle encompassing reflection points is 17 m. Sensing footprint for each reflection point is an ellipse with a major axis of ∼2× the radius at the reflection point (and minor axis of ∼4 m), resulting in a daily sensing footprint of ∼3600 m^2.

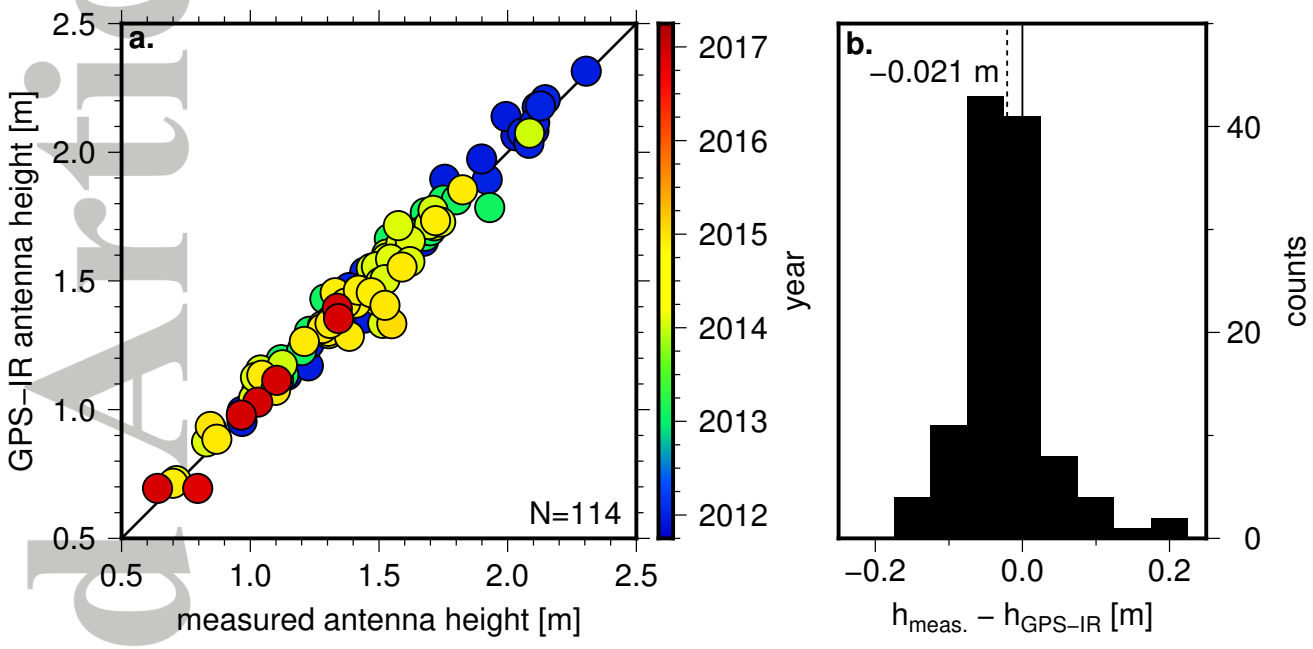

Figure 3. (a) Comparison between 114 in situ measurements of GPS antenna height and coincident GPS-IR estimate; color corresponds to time of field measurement. (b) Histogram of the difference between measured and GPS-IR-estimated antenna heights, showing approximately normally distributed residuals with a mean of -0.02 m.

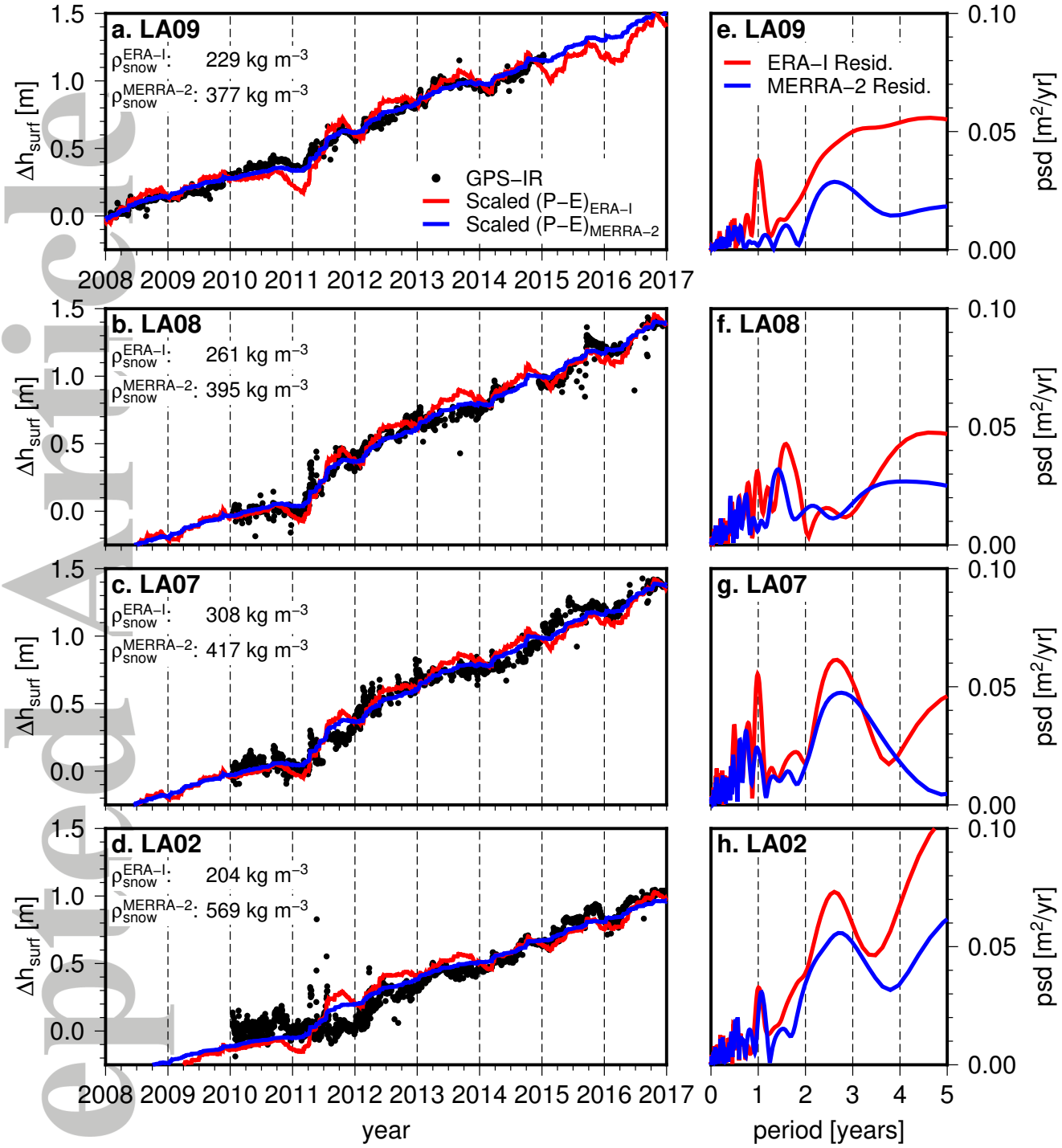

Figure 4. Seven-year time-series of surface-height change estimates at four GPS sites: (a) LA09, (b) LA08, (c) LA07, and (d) LA02 (see Figure 1 for locations), estimated from GPS-IR (black), ERA-Interim $P(t) - E(t)$ (blue), and MERRA-2 $P(t) - E(t)$ (red). Reanalysis products are scaled by best-fit ρ_{snow} noted, which minimizes the misfit in slope between each reanalysis product and GPS-IR observations. Power spectral densities of residuals between GPS-IR observation and ERA-Interim $P(t) - E(t)$ (red) and GPS-IR and MERRA-2 $P(t) - E(t)$ (blue) at (e) LA09, (f) LA08, (g) LA07, and (h) LA02.

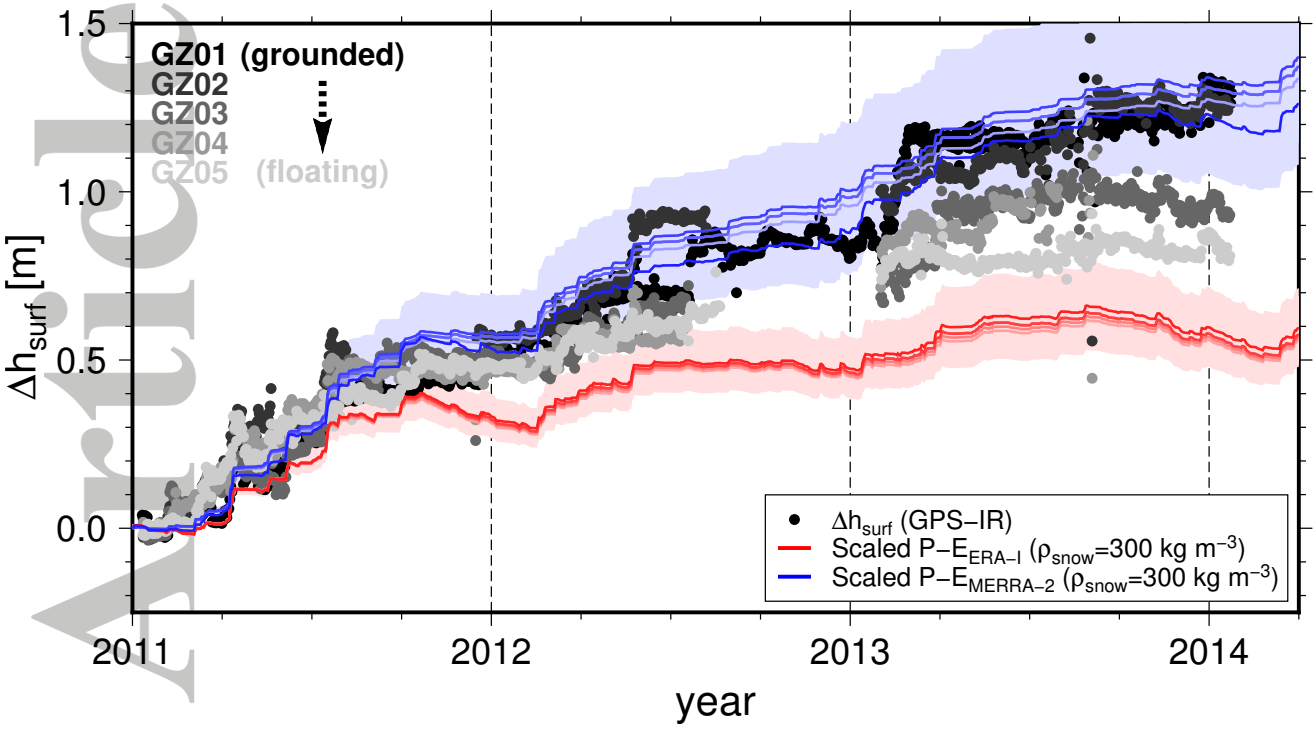

Figure 5. Three-year time-series of surface-height change estimates at five GPS locations along a 24-km transect that crosses the grounding line perpendicularly, spaced at ∼6 km intervals. Grey circles are GPS-IR surface-height change estimates, where shades of grey indicate location of site along the transect from fully grounded (GZ01, darkest) to fully floating (GZ05, lightest). Also shown are the values from the atmospheric models, ERA-Interim $P(t) - E(t)$ (shades of blue) and MERRA-2 $P(t) - E(t)$ (shades of red), where color intensity again denotes grounded (darkest) to floating (lightest) along the transect. Solid lines lines represent scaling by 300 kg m^{-3}, surrounded by a corresponding lightly colored region indicating the range of $P(t) - E(t)$ for a likely values of ρ_{snow} (250 to 350 kg m^{-3})